CHARACTERIZING THE IONOSPHERIC RESPONSE TO THE 2017 SOLAR ECLIPSE THROUGH RAYTRACING ANALYSIS

Magdalina Moses[a], Gregory Earle[a], Lee Kordella[a], Doug Drob[b], Joe Huba[b], Joshua Vega[c], Nathaniel Frissell[c]

[a]Virginia Tech, [b]Naval Research Laboratory, [c]New Jersey Institute of Technology

Abstract

On August 21, 2017 there was a total solar eclipse over the United States, offering an opportunity to study the dependence of the ionospheric density and morphology on incident solar radiation. There are significant differences between the ionospheric conditions during a solar eclipse and those normally experienced at sunset and sunrise, including the west-to-east motion of the eclipse terminator and the speed of the transition. Taken together, these factors imply that unique ionospheric responses may be witnessed during eclipses, reflected by changes in radio propagation. In order to study these changes, we ran the Super Dual Auroral Radar Network (SuperDARN) radars in Oregon and Kansas in a special mode on the eclipse day to enhance their data's temporal and spatial resolution. These data show distinct changes in propagation during the eclipse. In order to investigate the underlying processes governing the ionospheric response to the eclipse, we employ the high frequency propagation toolbox (PHaRLAP), created by Dr. Manuel Cervera, to simulate SuperDARN data for different models of the eclipsed ionosphere. By invoking different hypotheses and comparing simulated results to SuperDARN measurements we can study the underlying processes governing the ionosphere and improve our model of ionospheric responses to an eclipse.

Introduction

Physics of the Ionosphere

The electron density in the ionosphere varies with many factors including altitude and time of day among others. The ionosphere's density is very dependent on sunlight. Exclusive of plasma dynamics, the continuity equation for plasma production, q, and loss, is given by the equation: $\alpha\beta N^2 - \alpha q N - \beta q = 0$, where α and β are recombination coefficients and N is density[1]. During an eclipse, q will decrease dramatically as the solar disk is obscured. The imbalance between production and loss should result in a decrease in electron density during the eclipse, especially at lower altitudes.

At night all layers of the ionosphere experience a large decrease in electron density as shown in the figure below (Figure 1).

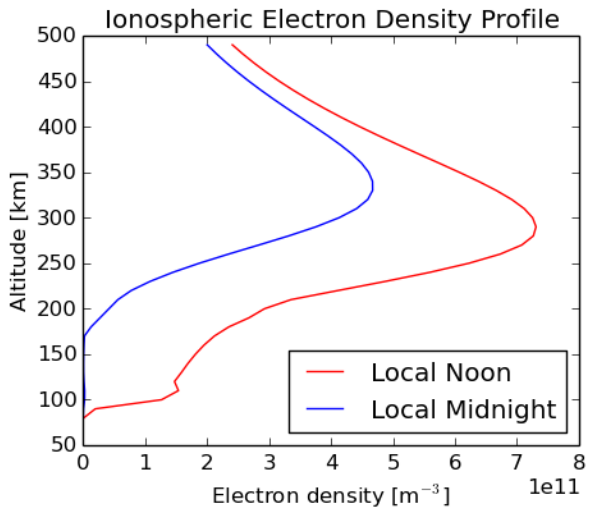

Figure 1. Day vs. Night Electron Density Profiles. During an eclipse, the ionosphere will evolve toward a nighttime density over a much shorter timescale.

The time scale at which the eclipse blocks most of the sunlight is much shorter than night and the corona is still visible during an eclipse. This suggests that the ionosphere will not experience the same magnitude decrease in electron density as at night. However, a decrease in density in the eclipsed region can be expected. Additionally, since the magnitude of the eclipse varies with location, some instabilities in the ionosphere could be generated due to variations in density.

Both changes in density and onset of plasma instabilities associated with eclipses may be detectable by monitoring changes in radio frequency (RF) propagation by ground-based systems.

Radio Wave Propagation

Radio waves propagation is governed by the medium in which the wave is traveling and the frequency of the wave. In the ionosphere, the density of the plasma determines the frequency threshold for propagation through the plasma. The critical frequency (f_p) in MHz and the plasma number density (N) in particles/cm^3 is approximately given by $f_p = 9x10^3 * \sqrt{N}$. If the frequency of a radio wave is greater than the critical frequency, then the wave will propagate through the region and escape the ionosphere, otherwise it will be refracted. The radio waves that are most impacted by the ionosphere are those in the high frequency (HF) band, approximately 3 MHz - 30 MHz. Additionally, the angle of incidence of a RF wave on a plasma layer also determines how a wave is refracted by the layer. Radio waves with a smaller angle of incidence are more likely to be bent back to Earth, when they encounter a layer of sufficiently dense plasma.

Propagation of radio waves can be modeled by ray-tracing where the radio wave is treated as a ray propagating through some region. The HF propagation toolbox (PHaRLAP)[2], created by Dr. Manuel Cervera, is a widely used raytracing tool that models propagation through a user-defined model ionosphere.

Figure 2, generated with PHaRLAP, illustrates the changes in propagation that a variation in plasma density induces. The top panel shows the paths associated with 14 MHz signals propagation at different initial elevation angles in a nominal mid-day ionosphere and the bottom plot shows the paths taken by the same rays through an ionosphere with a region of depleted plasma, or a hole in the plasma. As illustrated in the plots, rays with a sufficiently high angle of incidence are slightly refracted, but manage to escape the ionosphere. In the top plot, rays with a smaller angle of incidence, or lower initial elevation angle, are refracted back towards Earth. In the bottom plot, the lower initial elevation rays that pass through the depleted region are bent in

such a way that they travel parallel to the ground through the depleted region over a great distance. In other words, these rays are ducted through the depleted region.

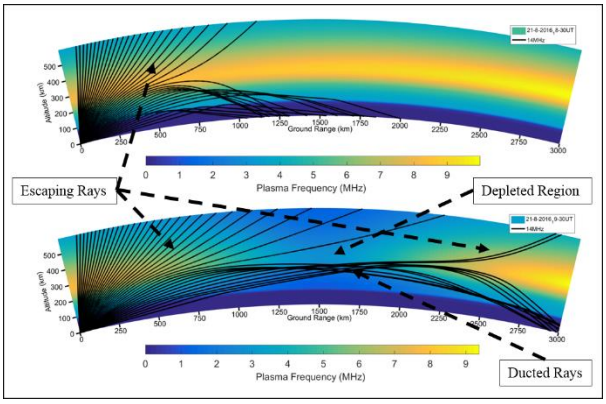

Figure 2. Ray-trace on 14MHz ray through unperturbed ionosphere (top) and through perturbed ionosphere with a region of depleted plasma density (bottom)

Thus, PHaRLAP is a useful tool in the prediction and analysis of eclipse-induced propagation effects.

Radar Systems

Radar is one of the most common method for measuring radio wave propagation through the ionosphere and extracting information on the ionospheric profile from these measurements. Ionospheric radar systems such as ionosondes typically send out a RF pulse signal and measure the time it takes for the signal to return. The distance the pulse traveled is then calculated from this time and the speed of light.

Historical Observations

Since the early-to-mid 1900s, researchers have conducted experiments to observe ionospheric phenomena that arise as effects of an eclipse. These results confirm the expectation that there is a significant decrease in the ionospheric electron density due to an eclipse.

The plot of Britain's Chilton ionosonde's foF2 data during the August 1999 eclipse (Figure 3) shows a significant decrease in foF2 at the onset of the eclipse (with totality at about 1000LT). This decrease is a distinct deviation from the IRI model for that date.

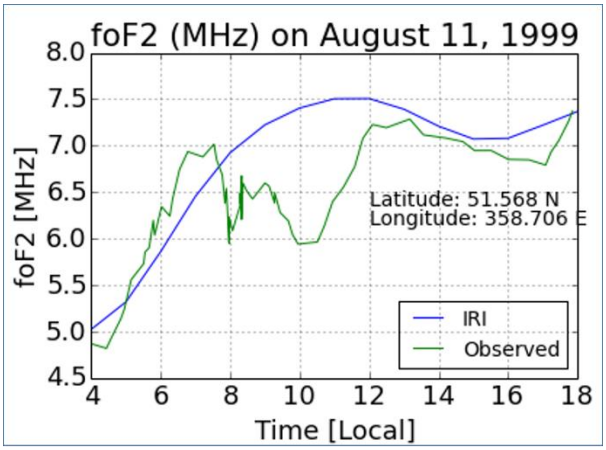

Figure 3. Effect of the August 11, 1999 eclipse on foF2[3]. The decrease in the observed foF2 (green) from the IRI model (blue) over a long period coincides with partial obscuration of the solar disk.

Results from other eclipses have indicated that there is also a large spatial effect on the ionosphere extending outside the eclipse's region of totality. For example, the Special Sensor Ultraviolet Spectrographic Imager (SSUSI) instrument observed a depleted airglow region roughly 1,000 km in diameter during a solar eclipse over western Africa.

A survey of past eclipse observations show some inconsistent results. It is likely that eclipses may be affected by magnetic latitude and other geophysical effects.

2017 Eclipse Experiment Overview

The August 21, 2017 total solar eclipse covered a very long longitudinal path over the US, unmatched by any eclipse over the US in the past 60 and in the next 30 years. The development of observational networks across the US, such as the Continuously Operating Reference Station (CORS) network, the Super Dual Auroral Radar Network (SuperDARN) and various amateur radio reporting networks, have enhanced the potential spatial and temporal resolution relative to previous studies.

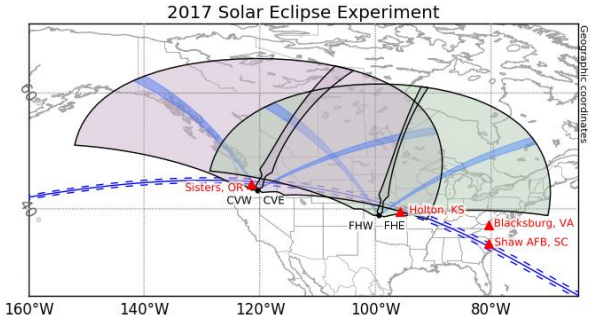

Figure 4. SuperDARN radars' fields of view (magenta and green) and Ionospheric sounders' locations (red triangles) relative to the eclipse's path of totality (blue).

Our research group established four temporary field stations using software defined radios (SDRs) with three stations along the path of totality and one station outside of totality as illustrated in Figure 4. These stations were vertical incidence sounders. Additionally, our experiment relied on two SuperDARN radars in Oregon and Kansas that had the eclipse path in their field-of-view as shown in Figure 4.

The focus of the research presented here is the analysis of the changes in RF propagation observed by the SuperDARN radar at Christmas Valley, Oregon over the course of the eclipse.

SuperDARN Eclipse Observations

SuperDARN slant range data gives the range (d) in kilometers (km) that the radar's signal traveled based on the time it took for the signal to return to the receiver (Δt) according to the equation $d = c/\Delta t$, where c is the speed of light in a vacuum. The slant range data from the Christmas Valley West (CVW) SuperDARN radar shows a distinct eclipse effect illustrated in the Figure 5.

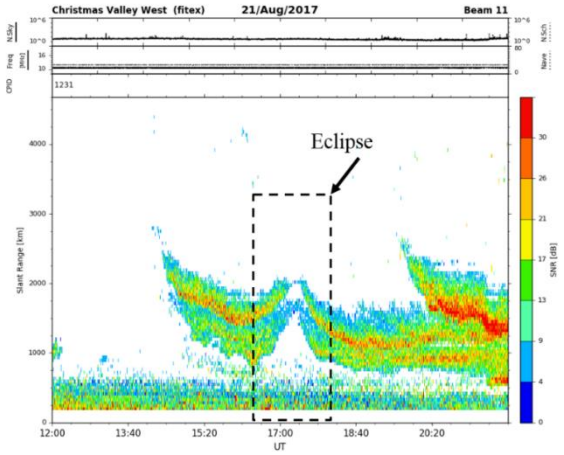

Figure 5. SuperDARN Christmas Valley West radar Range-Time-Intensity plot for the eclipse day.

Figure 5 shows that as the eclipse progresses, the radar signals go further out before they are reflected back towards the radar. Under normal conditions, this increase in slant range is often a signature of an upward motion in the ionospheric plasma. However, through ray tracing we were able to show that this is actually likely due to ducting effects as shown in Figure 6.

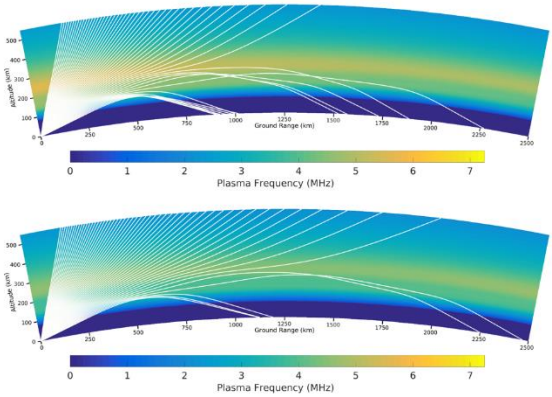

Figure 6. Ray-trace of a 10MHz ray through unperturbed ionosphere (top) and through eclipsed ionosphere (bottom)

Data Analysis

We developed a PHaRLAP-based 2D ray trace model of SuperDARN so that we could compare SuperDARN data to the output of the ray trace for different models of the eclipsed ionosphere. Models of the eclipsed ionosphere were generated by imposing different conditions on the Navel Research Lab's (NRL's) two-dimensional (SAMI2) and three-dimensional (SAMI3) SAMI (Sami is Another Model Ionosphere) models.

SAMI3 Models

We imported the output electron densities from our NRL collaborators' first SAMI3 model of the eclipsed ionosphere[4] into our SuperDARN simulation algorithm and generated the comparison of the SuperDARN measurement and the ray-trace simulated data shown in Figure 7. Although the modeled data agrees very well with the measured data on the onset phase of the eclipse, model data differs drastically from measured data during the recovery phase.

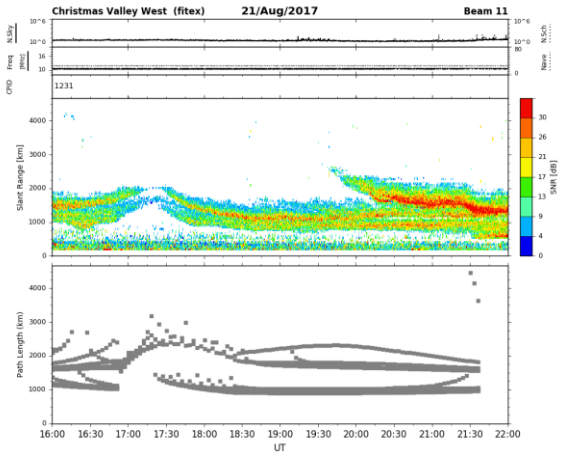

Figure 7. SuperDARN Christmas Valley West radar measured range data (upper) and ray-trace model data (lower).

During an internship at NRL, one of our group's members made improvements to the previous model, including an improved eclipse shadow function. As shown in Figure 8 below, simulated SuperDARN data using this new model agree better with measured data than those of the first SAMI3 model; however, the recovery time predicted by the model is still a too long. This suggests that some feature of the ionospheric response is not accurately represented.

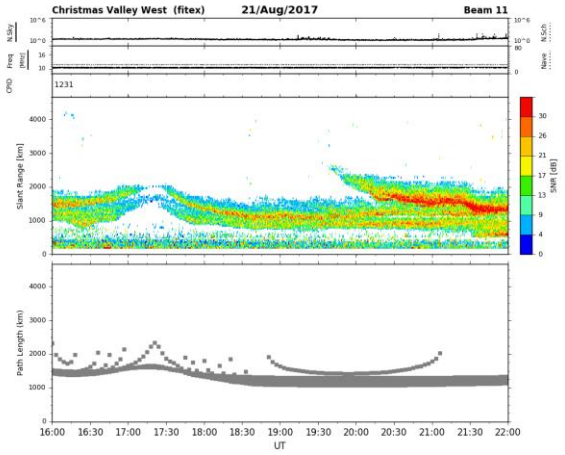

Figure 8. SuperDARN Christmas Valley West radar measured range data (upper) and ray-trace model data generated with new SAMI3 model (lower).

There are many parameters that could be modified in the SAMI3 eclipse model. As SAMI3 is computationally intensive, it would be time consuming to run multiple case studies in order to determine which case fits these measured eclipse data best. In order to expedite this selection, we examined the impacts of imposing certain conditions in the eclipsed 2D model of SAMI (SAMI2) on the ray-trace.

SAMI2 Wind Study

One of SAMI's input parameters that is most likely to be set to an inaccurate eclipse value is the neutral wind's velocity. SAMI takes neutral wind speed and direction values from NRL's Horizontal Wind Model (HWM), an empirical model of the upper atmosphere. However, the eclipsed atmosphere's wind velocity probably differed from that given by HWM for a normal day. As winds can have an impact on plasma motion, different values of wind speeds and directions in SAMI produce different ionospheric electron density models.

Methodology

For a preliminary study, we ran SAMI2 for four cases: no wind, default wind values from HWM, East/West wind values from HWM with no North/South wind, and North/South wind values from HWM with no East/West wind. The ray-trace profiles from the default HWM case for control and maximum eclipse conditions are shown in Figure 9.

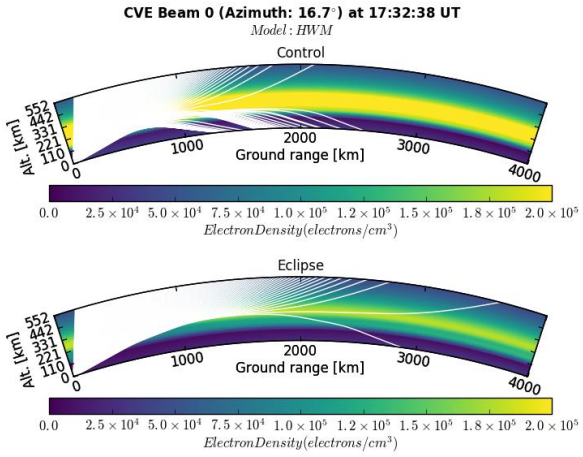

Figure 9. Ray-trace of a 10.5 MHz ray through unperturbed ionosphere (top) and through eclipsed ionosphere (bottom) at maximum eclipse.

Although ray-trace profile plots are a good way of comparing the propagation paths through the eclipsed and uneclipsed models at a single time, it is difficult to visualize the behavior of the model and ray-paths over time in this representation. In order to do this, we took the rays with the longest and shortest path lengths and found the midpoint value of the profile's path lengths by $l_{midpoint} = \frac{l_{long}+l_{short}}{2}$, where l_{long} is the largest path length, l_{short} is the smallest path length and $l_{midpoint}$ is the midpoint value. These midpoint values are plotted as circles in Figure 10 bellow, with the minimum and maximum path lengths indicated by the bars.

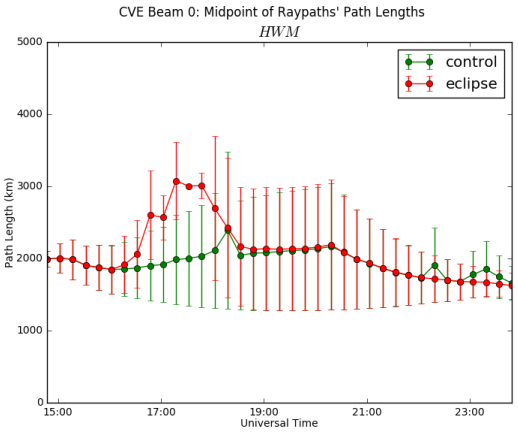

Figure 10. Midpoint and bounds of ray-path profile from ray-trace through output of SAMI2 model initialized with default HWM values.

From this, we can see that the path lengths of the rays generally increase around the time of the eclipse, but then quickly return to the path lengths of the control case after the eclipse is over, with a few deviations hours after the eclipse.

Preliminary Results

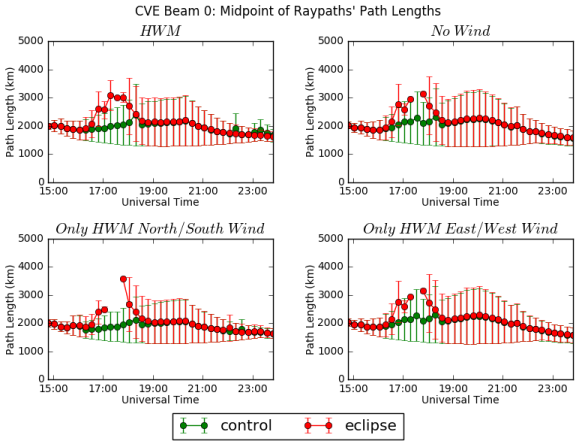

Figure 11. Plots of midpoint and bounds of ray-path profile from ray-trace through output of SAMI2 models initialized with four different wind models.

The bounds and midpoint values of the path lengths generated by ray-traces through the models generated by each of the four cases are shown in the subplots of Figure 11. The “only east/west wind” plot does not appear to be significantly different from the “no wind” plot in either the eclipse or control cases. In contrast, the “only north/south wind” plot and the “only east/west wind” plot with the “no wind” plot appear to differ significantly in the eclipse case and to differ slightly in the control case. This suggests that the ionosphere may be more sensitive to eclipse-induced variations in the north-west wind rather than the east/west wind.

Conclusion and Future Work

The study of the ionospheric response to the 2017 total solar eclipse incorporates data from several radio instruments including SuperDARN and temporary radio sounder sites. The focus of the research presented here is the ionospheric response observed by the CVW SuperDARN radar in Oregon. CVW observed a distinct increase in the range of radio signals over the course of the eclipse, peaking around totality. Raytracing models indicate this phenomena is due to ducting of the radio waves in the eclipse-induced, plasma depleted region of the ionosphere. Analysis of the underlying ionospheric physics consists of comparison of SuperDARN data with simulated SuperDARN data, obtained by raytracing. Initial models showed good agreement between measured and modeled data during the onset phase of the eclipse. However, there is significant disagreement between simulated and measured data during the recovery phase. One possible reason for this discrepancy could be incorrect values for the neutral wind’s magnitude and direction during the eclipse. In order to investigate the neutral wind’s effects on the eclipse model, we implemented several cases in SAMI2 and ray-traced through the output. Preliminary results indicate that the

North/South wind probably has a larger impact on the modeled eclipse response than does the East/West wind; however, more case studies are necessary to confirm this result. Future work will include further case studies on the impact of the direction of the wind as well as the impact of changing the magnitude of the wind's speed.

References

1. Rishbeth, H.; Garriott, O. K., *Introduction to Ionospheric Physics*. Academic Press Inc. : New York; San Francisco; London, 1969.
2. Cervera, M. A.; Harris, T. J. In *Modelling the effects of ionospheric disturbances on quasi-vertically incident ionograms using 3D magneto-ionic raytracing*, 2011 XXXth URSI General Assembly and Scientific Symposium, 13-20 Aug. 2011; 2011; pp 1-4.
3. Afraimovich, E. L.; Kosogorov, E. A.; Lesyuta, O. S., Effects of the August 11, 1999 total solar eclipse as deduced from total electron content measurements at the GPS network. *Journal of Atmospheric and Solar-Terrestrial Physics* **2002,** *64* (18), 1933-1941.
4. Huba, J. D.; Drob, D., SAMI3 prediction of the impact of the 21 August 2017 total solar eclipse on the ionosphere/plasmasphere system. *Geophysical Research Letters* **2017,** *44* (12), 5928-5935.

The ray tracing results presented in this paper were obtained using the HF propagation toolbox, PHaRLAP, created by Dr. Manuel Cervera, Defence Science and Technology Organisation, Australia (manuel.cervera@dsto.defence.gov.au). This toolbox is available by request from its author.